On the sensitivity analysis of angle-of-attack in a model reduction setting

Hay, Alexander; Akhtar, Imran; Borggaard, Jeff

AIAA, 2010-1473, 2010-01-04

48th AIAA Aerospace Sciences Meeting Including the New Horizons Forum and Aerospace Exposition
4 - 7 January 2010, Orlando, Florida

AIAA 2010-1473

On the Sensitivity Analysis of Angle-of-Attack in a Model Reduction Setting

Alexander Hay*, Imran Akhtar† and Jeff T. Borggaard‡

Interdisciplinary Center for Applied Mathematics, Virginia Tech, Blacksburg, VA 24061, USA

The proper orthogonal decomposition (POD) based model reduction method has been successfully used in fluid flows. However, the main drawback of this methodology rests in the robustness of these reduced-order models (ROMs) beyond the reference, from which POD modes have been derived. Any variation in the flow or shape parameters within the reduced-order model fails to predict the correct dynamics of the flow field. To broaden the spectrum of these models, the POD modes should have the global characteristics of the flow field over which the predictions are required. Mixing of snapshots with varying parameters is one way to improve the global nature of the POD modes but has shown limited success. Instead, we have used Sensitivity Analysis to include the flow and shape parameters influence within POD modes and developed robust reduced-order models for varying viscosity (Reynolds number), changing orientation and physical deformation of the bodies. In this study, we address the flows over an elliptic cylinder for a range of incidence angles. We use Sensitivity Analysis to develop reduced-order models and show their capabilities in capturing the effect of varying inflow and predicting the dynamics of the flow field.

I. Introduction

Most of the fluid flows are governed by partial differential equations (PDEs) which correspond to an infinite number of degrees of freedom in the system; Navier-Stokes is one such example. The analytical solution exists only for a limited number of simple flows. These equations are typically solved using computational fluid dynamics (CFD); however, for complex flows the degrees of freedom may still be in thousands or even in millions. Many engineering and industrial problems involving fluid-structure interaction require repeated simulations of unsteady fluid flows. From a practical point of view, it is often impossible to perform these simulations for a variety of parameter values required for design, control, and optimization. Thus, reduced-order model techniques are often employed to build dynamical systems having a reduced number of degrees of freedom that approximate complex physical problems and minimize the computational cost.

The proper orthogonal decomposition (POD)-Galerkin approach is often used to develop reduced-order models for the fluid flows. This methodology requires snapshots of the flow field either from an experiment or a numerical simulation. In the first step, POD modes are computed using the snapshot data.[1–3] Next, the velocity field is written as the sum of the mean flow ($\bar{\mathbf{u}}$) and the velocity fluctuations ($\mathbf{u}'$). The mean flow $\bar{\mathbf{u}} = \langle \mathbf{u} \rangle$, where $\langle\rangle$ is the time average of the assembled data, is subtracted from $\mathcal{W}$. Then, the fluctuations are expanded in terms of the POD eigenfunctions (Φ_i) as follows:

$$\mathbf{u}(\mathbf{x}, t) \approx \bar{\mathbf{u}}(\mathbf{x}) + \sum_{i=1}^{M} q_i(t)\Phi_i(\mathbf{x}), \tag{1}$$

where M is the number of POD modes used in the projection. Substituting the velocity in the governing equations (e.g. Navier-Stokes equations) gives a reduced-order model of the form:

$$\dot{\mathbf{q}} = \mathbf{F}(\mathbf{q}) \tag{2}$$

*Current Address: Industrial Materials Institute, National Research Council Canada, Boucherville, QC, Canada J4B 6Y4.
†Postdoctoral Associate.
‡Professor, Department of Mathematics.

Depending on the problem, the number and variety of snapshots used to generate the POD modes can have a strong influence on the general applicability of the reduced-order model. Despite the accuracy of the model at this specific Reynolds number, the model lacks robustness away from the reference simulation. Deane *et al.*[4] note that *the accuracy of the model predictions rapidly deteriorate as we move away from the decomposition value*. Obviously, the accuracy of reduced-order models depends on how well the POD basis can represent the desired set of solutions. In this case, the accuracy of the model is good only in the parameter value of the reference simulation from which POD basis are derived. Deviation in any parameter, within the reduced-order framework, will compromise the accuracy of the model and may lead to instability of the model. In addition, POD-based models have limitations in predicting bifurcations in control parameter variation if the snapshot data does not contain the qualitative change in the range of parameter over which bifurcation occurs. Ma and Karniadakis[5] investigated the stability and dynamics of three dimensional limit-cycle states for the flow past a cylinder using low-dimensional modeling. They mixed the snapshot data before and after the Mode A[6] instability to predict the jump in the Strouhal number vs Reynolds number curve. Noack *et al.*[7] suggested a generalization for POD based Galerkin models to include the transient behavior. In their Galerkin approximation, they included an additional vector and termed it a *shift-mode*. The approaches of adding shift-modes and mixing the snapshots to capture the flow physics in a wide range are encouraging and expand the application of POD based reduced-order models.

In our previous work,[8,9] we proposed the inclusion of derivatives of the POD basis functions (computed using Sensitivity Analysis). The study considered two approaches for using the POD derivatives to define an improved reduced basis. In the first approach, we used linear extrapolation in the parameter space of the standard POD basis (*extrapolated basis*); while in the second approach, we combined the POD and POD derivatives to construct an expanded basis (*expanded basis*) suited to account for a larger range of parameter values. The underlying idea behind this approach is that the POD mode sensitivities span a different subspace than the one generated by the POD eigenfunctions. Furthermore, this subspace is deemed appropriate to represent changes in solutions with parameter variations. Both approaches have led to improved reduced-order models in the study of flow past a square cylinder where the viscosity (equivalently, the Reynolds number) was varied from the reference value. However, when considering larger parameter changes, the expanded approach was demonstrated to provide a much more robust strategy. In particular, it was shown that it converges to a stable limit cycle that is a fairly good approximation of the attractor of the full-order simulation even for large parameter changes. This previous study was limited to problems with fixed geometries by considering only value parameters. Follow up studies extended the proposed approaches to shape (or design) parameters (*i.e.* parameters that define the geometry of the problem.) We demonstrated our shape sensitivity analysis approaches by developing reduced-order models for flows where the parameter described: 1) the orientation of a square cylinder placed in a channel (10, 11); 2) the thickness ratio of an elliptic cross-section cylinder (12, 13). In the first case, POD mode sensitivities where computed using flow data obtained by the Sensitivity Equation Method and differentiation of the eigenvalue problem. In the second case POD modes where calculated by a finite-difference approach. In both cases, it has been shown that the *extrapolated* and *expanded* bases yield more robust reduced-order approximations and hence that the inclusion of shape sensitivity information in the POD bases performs better than the baseline approach (one on one mapping without the inclusion of sensitivity). However, a limitation has also been uncovered since the expanded basis has led to ROM having incorrect behaviors (note that the extrapolated approach is not subjected to this problem). The most striking example is observed at the baseline where energy is transferred from the POD modes to their sensitivities though the latter components should not be activated at all. The present work aims at extending the methods to varying inflow conditions.

II. Numerical Methodology

A. Model equations

We consider flows described by the unsteady incompressible Navier–Stokes equations. The momentum and mass conservation laws are written as :

$$\rho\frac{\partial \mathbf{u}}{\partial t} + \rho(\mathbf{u}\cdot\nabla)\mathbf{u} = \nabla\cdot\boldsymbol{\sigma}, \tag{3}$$

$$\nabla\cdot\mathbf{u} = 0 \tag{4}$$

where $\mathbf{u}$ is the velocity vector and $\boldsymbol{\sigma} = (-p\mathbf{I} + \boldsymbol{\tau}(\mathbf{u}))$ is the stress tensor, ρ the density, p the pressure and $\mathbf{I}$ the second-order identity tensor. For Newtonian fluids, the viscous stress tensor is given by :

$$\boldsymbol{\tau}(\mathbf{u}) = \mu \left(\nabla \mathbf{u} + (\nabla \mathbf{u})^T \right) \tag{5}$$

where μ is the fluid viscosity. The solution to these equations is sought on a domain Ω with a boundary $\Gamma = \Gamma_D \cup \Gamma_N$ and over times $t \in \mathcal{T} = (0, t_f)$. Dirichlet and homogeneous Neumann boundary conditions are imposed on boundary segments Γ_D and Γ_N, respectively :

$$\mathbf{u} = \overline{\mathbf{u}} \qquad (\Gamma_D), \tag{6}$$

$$\boldsymbol{\sigma} \cdot \hat{\mathbf{n}} = \mathbf{0} \qquad (\Gamma_N), \tag{7}$$

where $\hat{\mathbf{n}}$ is an outward unit vector normal to the boundary. The variables are initialized in time using a prescribed initial solution.

For both the DNS and the ROM simulations of this PDE, the weak-forms of (3) and (4) are formed by a Galerkin projection on a set of suitable test functions. In particular, the test functions for the momentum equation satisfy the homogeneous version of the Dirichlet boundary conditions (6) (i.e $\mathbf{w} \in \mathbf{X_0} = \{\mathbf{f} \in \left[H^1(\Omega)\right]^d \,|\, \mathbf{f} = \mathbf{0} \text{ on } \Gamma_D\}$ with d the dimension of the problem). Then, we seek $\mathbf{u} \in \mathbf{X} = \left[H^1(\Omega)\right]^d$ and $p \in L^2_0(\Omega)$ such that

$$\int_\Omega \left(\rho \frac{\partial \mathbf{u}}{\partial t} + \rho(\mathbf{u} \cdot \nabla)\mathbf{u} \right) \cdot \mathbf{w} \, d\Omega = \int_\Omega p \, (\nabla \cdot \mathbf{w}) - \boldsymbol{\tau} : \nabla \mathbf{w} \, d\Omega \qquad \forall \, \mathbf{w} \in \mathbf{X_0}, \tag{8}$$

$$\int_\Omega q \, (\nabla \cdot \mathbf{u}) \, d\Omega = 0 \qquad \forall \, q \in L^2_0(\Omega). \tag{9}$$

These equations have been obtained by integrating by parts the term involving $\boldsymbol{\sigma}$ as classically done :

$$\int_\Omega (\nabla \cdot \boldsymbol{\sigma}) \cdot \mathbf{w} \, d\Omega = \int_\Gamma (\boldsymbol{\sigma} \cdot \mathbf{w}) \cdot \hat{\mathbf{n}} \, d\Gamma - \int_\Omega \boldsymbol{\sigma} : \nabla \mathbf{w} \, d\Omega \tag{10}$$

$$= \int_\Gamma (\boldsymbol{\sigma} \cdot \hat{\mathbf{n}}) \cdot \mathbf{w} \, d\Gamma + \int_\Omega p \, (\nabla \cdot \mathbf{w}) - \boldsymbol{\tau} : \nabla \mathbf{w} \, d\Omega. \tag{11}$$

The integrand in the boundary integral is zero on Γ_D since $\mathbf{w} \in \mathbf{X_0}$ and also on Γ_N from the homogeneous Neumann boundary condition (7). For the DNS, the test functions are finite-element interpolation functions that span $\left[H^1(\Omega)\right]^d$ (see § B); for the ROM, the test functions are the global modes that span the space generated by the baseline flow (and possibly sensitivity) snapshots.

B. Flow description and Direct Numerical Simulation

We consider here two-dimensional flows ($d = 2$) over an elliptic cylinder having a semimajor axis along the x-axis (L_x) twice as large as its semiminor axis along the y-axis (L_y). Solutions are sought for a range of angles of incidence α of the incoming free-stream flow (see Eq. (6)) $\overline{\mathbf{u}} = [\cos(\alpha), \sin(\alpha)]^T$. The Reynolds number based on the semimajor axis length and the free-stream velocity $U_\infty = ||\overline{\mathbf{u}}||$ ($Re = \rho U_\infty L_x / \mu$) is set to 200 so that all flows examined in this study are reported to be two-dimensional, laminar and T-periodic in time exhibiting a Von Kármán vortex street.

As can be seen in figure 1, the computational domain Ω extends $15D$ away from the rear cylinder edge to allow for the simulation of the convection of several vortexes in the wake of the cylinder. The inflow and sides of the computational domain are located six edge lengths away. The boundary conditions on $\Gamma = \Gamma_D \cup \Gamma_N$ are set as follows. At the inlet and cylinder edges (Γ_D), Dirichlet boundary conditions are applied; the no-slip condition holds on the cylinder walls ($\overline{\mathbf{u}} = [0, 0]^T$) and the free-stream velocity ($\overline{\mathbf{u}} = [\cos(\alpha), \sin(\alpha)]^T$) is prescribed at the inlet. At the sides and outlet of the computational domain (Γ_N), the homogeneous Neumann boundary condition is applied as described by (7).

The DNS is performed by solving the discretized version of equations (8)-(9) using the Taylor-Hood ($P_2 - P_1$) finite-element and a mixed-formulation. Thus, the velocity variables are discretized by 6-noded

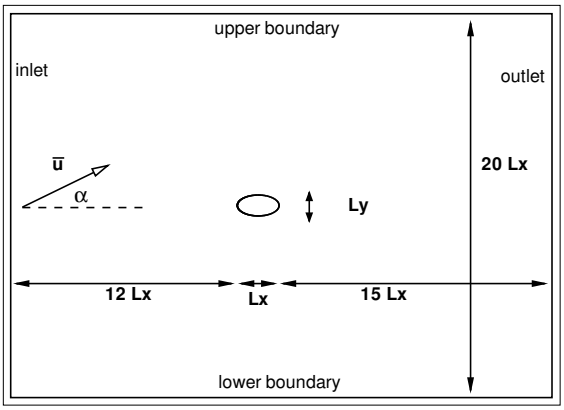

Figure 1. Computational configuration

quadratic interpolation functions (third-order spatial accuracy) while the pressure is discretized by piecewise linear continuous functions (second-order spatial accuracy). An implicit Crank-Nicolson time discretization of these equations (second-order temporal accuracy) leads to a system of nonlinear algebraic equations which are linearized by Newton's method and solved using a sparse direct solver.

The mesh is defined by an adaptive refinement procedure used for solving the steady-state equations for the baseline flow. Additional user-defined uniform refinement is applied in the wake region to allow for the accurate calculation of the vortex street in the unsteady calculations. The resulting mesh contains $43,000$ nodes and is illustrated in Fig. 2. Furthermore, the non-dimensional time step for the integration scheme is 0.01. Several refinement studies for both the space and time discretizations indicate sufficient numerical accuracy.

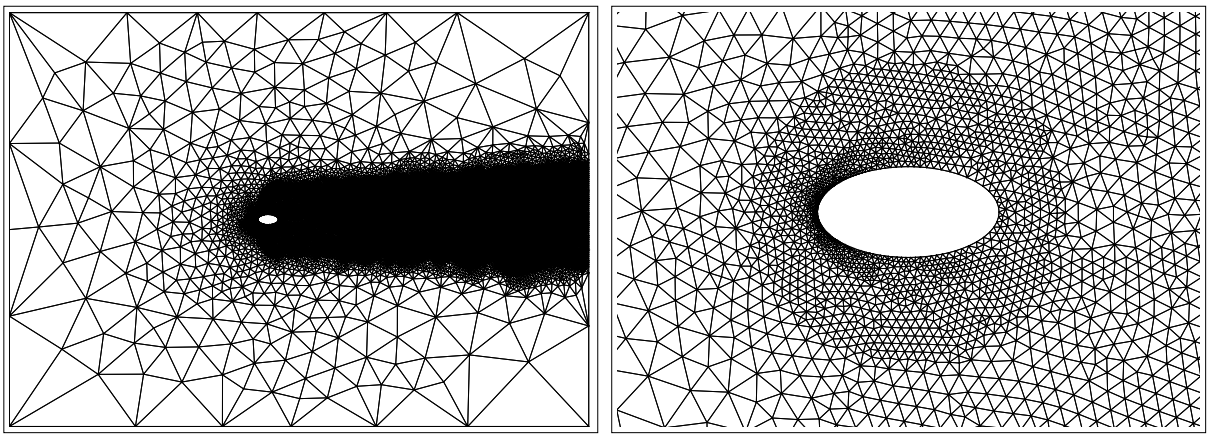

Figure 2. Computational mesh

The DNS solution is initialized by prescribing the solution of the steady version of (3)-(4). During the first instant of the calculation, a continuous perturbation is imposed to the inflow condition to speed up the onset of the vortex shedding.

The numerical results have been validated by comparing the Strouhal number ($St = fD/U_\infty$ where f is the vortex shedding frequency) and mean drag and lift coefficient on cylinders with different cross-sections and at several Reynolds number and incidences to those in the literature as reported in 9, 10.

III. POD-Galerkin Reduced-Order Model

A. The proper orthogonal decomposition

Mathematically, we compute Φ for which the following quantity is maximum:

$$\frac{\left\langle |(\mathbf{u}, \Phi)|^2 \right\rangle}{\|\Phi\|^2}, \tag{12}$$

where $\langle . \rangle$ denotes the ensemble average. Applying variational calculus, one can show that Equation (12) is equivalent to a Fredholm integral eigenvalue problem represented as

$$\int_\Omega R_{ij}(\mathbf{x}, \mathbf{x}')\Phi^j(\mathbf{x}')\, \mathrm{d}\mathbf{x}' = \lambda \Phi^j(\mathbf{x}), \tag{13}$$

where i, j are the number of velocity components and $R(\mathbf{x}, \mathbf{x}')$ is the two-point space-time correlation tensor.

In the classical POD or direct method, originally introduced by Lumley,[1] R_{ij} is a two-point spatial-correlation tensor and the eigenfunctions are the POD modes. In this approach, the average operator is estimated in time. On the other hand, if the average operator is evaluated as a space average over the domain of interest, the method is known as the method of *snapshot*.[3] In this approach, we formulate a temporal-correlation function from the snapshots and transform it into an eigenvalue problem as follows:

$$C_{ij} = \left\langle (\mathbf{u}^i, \mathbf{u}^j) \right\rangle, \tag{14}$$

where $(a, b) = \int_\Omega a.b\, \mathrm{d}\Omega$ represents the inner product between a and b. The POD modes are then computed by solving the eigenvalue problem

$$\mathbf{CQ} = \mathbf{Q}\lambda \tag{15}$$

where $\mathbf{Q}$ and λ are the eigenvectors and eigenvalues, respectively. Since $\mathbf{C}$ is non-negative Hermitian, $\mathbf{Q}$ is orthogonal by definition. The POD modes are computed as follows:

$$\Phi_i = \frac{1}{\sqrt{\lambda_i}} \mathcal{W} Q_i \tag{16}$$

An important characteristic of these modes is orthogonality; that is, $\Phi_i.\Phi_j = \delta_{ij}$, where δ_{ij} is the kronecker delta. The optimality of the POD modes lies in capturing the greatest possible fraction of the total kinetic energy for a projection onto the given set of modes.

The flow data or *snapshots* of the steady-state velocity field are sampled with a constant time interval (ΔT_s). The velocity field data (u, v) are assembled in a matrix $\mathcal{W}_{2N \times S}$, as follows:

$$\mathcal{W} = \begin{bmatrix} u_1^{(1)} & u_1^{(2)} & \dots & u_1^{(S)} \\ \vdots & \vdots & & \vdots \\ u_N^{(1)} & u_N^{(2)} & \dots & u_N^{(S)} \\ v_1^{(1)} & v_1^{(2)} & \dots & v_1^{(S)} \\ \vdots & \vdots & & \vdots \\ v_N^{(1)} & v_N^{(2)} & \dots & v_N^{(S)} \end{bmatrix} \tag{17}$$

Each column represents one time instant or a *snapshot* and S is the total number of snapshots for N grid points in the domain. The vorticity field can also be used for POD, however, in the case of the velocity field, the eigenvalues of $\mathcal{W}$ are a direct measure of the kinetic energy in each mode. Deane et al.[4] observed that 20 snapshots are sufficient for the construction of the first eight eigenfunctions at $\mathrm{Re}_D = 100 - 200$. In general, numerical studies[14] suggest that the first M POD modes, where M is even, resolve the first $M/2$ temporal harmonics and require $2M$ number of snapshots for convergence.

We write the velocity field as the sum of the mean flow ($\bar{\mathbf{u}}$) and the velocity fluctuations ($\mathbf{u}'$). The mean flow $\bar{\mathbf{u}} = \langle \mathbf{u} \rangle$, where $\langle \rangle$ is the time average of the assembled data, is subtracted from $\mathcal{W}$. Then, the fluctuations are expanded in terms of the POD eigenfunctions (Φ_i) following Eq. 1 Singular value decomposition (SVD) of this matrix provides the divergence-free velocity POD modes (Φ_i).

B. Reduced-order model by Galerkin projection

Using (1) and the fact that the POD is applied to an input collection that satisfies homogeneous Dirichlet boundary condition on Γ_D and is divergence free. By linearity, these properties are transmitted to the POD basis vectors. Hence, taking $\mathbf{w} = \boldsymbol{\phi}_i$ for $i = 1, \ldots, M$ in (8)-(9), one obtains :

$$\int_\Omega \left(\rho \frac{\partial \mathbf{u}}{\partial t} + \rho(\mathbf{u} \cdot \nabla)\mathbf{u} \right) \cdot \boldsymbol{\phi}_i \, d\Omega = - \int_\Omega \boldsymbol{\tau}(\mathbf{u}) : \nabla \boldsymbol{\phi}_i \, d\Omega \qquad \text{for} \quad i = 1, \ldots, M. \tag{18}$$

Note that the incompressibility constraint (9) is automatically satisfied since each $\boldsymbol{\phi}_j$ is solenoidal in the decomposition (1), and its associated Lagrange multiplier, the pressure, is eliminated from (8) or (11). Using the orthogonal decomposition in the set of M equations (18) leads to a set of ODEs for the time coefficients $\mathbf{q} = [q_1, \ldots, q_M]^T$ in the form of Eq. (2). In the present study, (2) is integrated in time using the explicit forth-order Runge-Kutta scheme. Moreover, accurate initial conditions can be obtained from the DNS data.

IV. Sensitivity Analysis

This section aims at deriving the first-order total derivatives of the POD modes with respect to a generic parameter α. This is referred to as the sensitivities of the POD vectors. In this study, they are computed by a second-order centered finite-difference (FD) approximation :

$$\left. \frac{D\Phi_i}{D\alpha}(\mathbf{x}(\alpha_0); \alpha_0) \right|_{FD} = \frac{\Phi_i(\mathbf{x}(\alpha_0 + \Delta\alpha); \alpha_0 + \Delta\alpha) - \Phi_i(\mathbf{x}(\alpha_0 - \Delta\alpha); \alpha_0 - \Delta\alpha)}{2\Delta\alpha}, \tag{19}$$

where α_0 is the parameter value at which the sensitivities are computed and $\Delta\alpha$ is the step in the finite-difference scheme. $\frac{D.}{D\alpha}$ represent the total derivative with respect to α. The parameter increment $\Delta\alpha$ is chosen sufficiently small for the FD computation to be accurate and sufficiently large for the difference between the two nearby POD vectors to be at least one order of magnitude larger than the discretization error.

The traditional approach in reduced-order modeling is to build the POD basis for one particular value of the parameter of the system. It will be referred to as the baseline value, noted α_0, which defined the baseline state, solution and POD basis. We aim at producing reduced-order solutions at perturbed states for $\alpha = \alpha_0 + \Delta\alpha$. To do so, we first considered the following bases :

- *Baseline POD basis* (BL) : This is the classical approach where the POD basis built from the data at the baseline state α_0 is used in Eq. (1) to subsequently produce a reduced-order model at the perturbed state α. These spatial modes are only available on the baseline geometry but they can easily be mapped on the perturbed geometry.

- *Perturbed POD basis* (PR) : the reduced-order model is constructed by using the POD modes extracted from the solution data obtained by a full-order simulation at the perturbed state α. This is a costly approach since each new reduced-order simulation at a new state required full-order data at this state. Thus, it has little interest in practice but will be used in the remainder of this study as a reference low-dimensional solution.

Following previous studies for value parameters in Ref. 8, 9 and shape parameters in Ref. 10, 11, 13, we examine two different ideas for constructing improved reduced-order bases using the Lagrangian sensitivity of the POD modes at the baseline state :

- *Extrapolated basis* (ET) : we treat each POD mode as a function of both space and parameter α : $\Phi_i = \Phi_i(\mathbf{x}; \alpha)$. A change $\Delta\alpha$ in the parameter from its baseline value α_0 is reflected in the modes through a first order expansion in the parameter space :

$$\Phi_i(\mathbf{x}; \alpha) = \Phi_i(\mathbf{x}(\alpha_0); \alpha_0) + \Delta\alpha \frac{D\Phi_i}{D\alpha}(\mathbf{x}(\alpha_0); \alpha_0) + O(\Delta\alpha^2). \tag{20}$$

  The effectiveness of this approach clearly depends on whether or not the POD modes exhibit a nearly linear dependence with respect to the parameter α. However, the dimension of the reduced basis is preserved and the reduced approximation of the solution variables still expressed using Eq. (1). Once again, the spatial functions are only available on the baseline geometry over which they have been computed but they can be mapped on the perturbed geometry.

- *Expanded basis* (EP) : the sensitivities of the modes can be shown to span a different subspace than the POD modes (see e.g. Ref. 8). Thus, it is natural to expect that if the approximated solution is selected in the union of the two subspaces generated by the POD modes and their sensitivities a broader class of solutions can be represented. It amounts to expand the baseline basis constituted of the M first eigenfunctions with their M sensitivities : $\left[\phi_1;\ldots;\phi_M;\frac{D\Phi_1}{D\alpha};\ldots;\frac{D\Phi_M}{D\alpha}\right]$. The underlying assumption behind this approach is that the subspace spanned by the mode sensitivities is well-suited to address the change in the solutions induced by a change in the parameter. However, the dimension of the reduced basis has doubled and the reduced approximation of the flow variables is now expressed from :

$$\mathbf{u}(\mathbf{x},t) \approx \bar{\mathbf{u}}(\mathbf{x}) + \sum_{i=1}^{M} q_i(t)\Phi_i(\mathbf{x}) + \sum_{i=M+1}^{2M} q_i(t)\frac{D\Phi_i}{D\alpha}(\mathbf{x}). \tag{21}$$

V. Results and Discussion

A. POD and Sensitivity Analysis

In what follows, all reduced-order models and approximations will be trained and built at the *baseline* state defined for the angle-of-attack $\alpha = 5^\circ$. They will be used to predict flows for incidences ranging from 0° to 10° (*i.e.* $\Delta\alpha = \pm 5^\circ$.)
During one vortex shedding cycle at the baseline, $m = 58$ snapshots of the FE solutions were collected to build the snapshot data matrix. The fluctuating kinetic energy captured by the POD modes is illustrated by plotting the POD spectrum on a logarithmic scale in Fig. 3(a). There is a rapid decrease in the energy

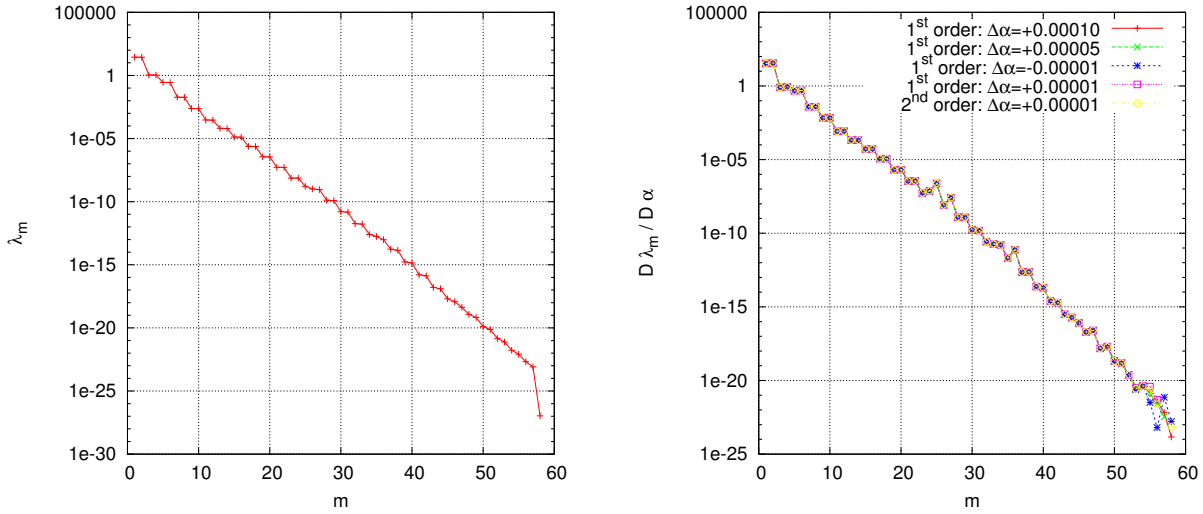

(a) POD spectrum

(b) Finite-difference sensitivities

Figure 3. POD spectrum and its FD sensitivity at baseline ($\alpha = 5^\circ$)

distribution so that the effectiveness of the POD is rapidly large. Figure 3(b) shows the values of the sensitivity of the POD eigenvalues. For verification purposes, we compare sensitivities computed by several finite-differences (first and second-order for different steps in the finite-difference.) As can be seen, the agreement between FDs is very good showing that the finite-difference calculation has converged. Note that the eigenvalue sensitivity decreases with the mode number in a (roughly) similar way as the eigenvalues do. This shows that the ordering of the eigenvalues will be preserved through changes in the parameter. Finally, the order of magnitude of the eigenvalue sensitivities is similar to that of their corresponding eigenvalues.

Figure 4 shows the contours of the streamwise and normal components of the first three spatial POD vectors at the baseline having a odd spectral number. Clearly, the POD modes are almost even or odd functions in y as it is the case for the symmetric configuration at no incidence ($\alpha = 0^\circ$) as reported in the literature. Here, given that the baseline configuration is asymmetric, this is only approximately true. However, the POD modes can still be grouped by pairs (hence we have only shown modes having a odd

spectral number), as for symmetric configurations, since this property comes from the temporal periodicity of the flows, which here is preserved through any parameter change, and makes the temporal eigenfunctions Fourier modes (see 8 for details). This is also the reason why the eigenvalues decay pairwise in Fig. 3(a).

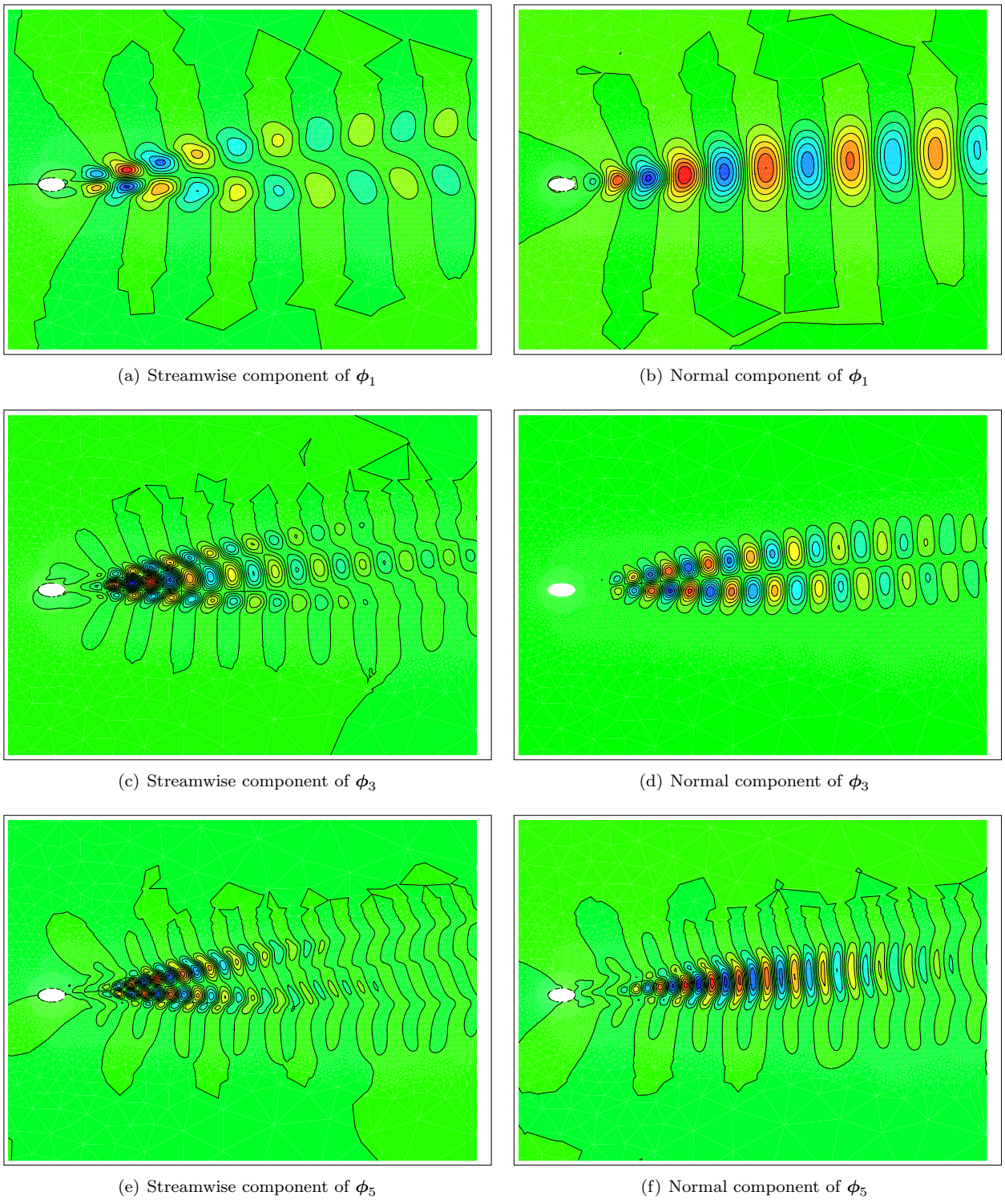

(a) Streamwise component of ϕ_1

(b) Normal component of ϕ_1

(c) Streamwise component of ϕ_3

(d) Normal component of ϕ_3

(e) Streamwise component of ϕ_5

(f) Normal component of ϕ_5

Figure 4. Iso-lines of the components of three baseline POD modes

A qualitative picture of the structure of the POD mode sensitivities is given in Fig. 5 where contours of the streamwise and normal components of the first three POD mode sensitivities with odd spectral number

are presented. Clearly, they contain different structures than the original POD modes. The sensitivities shown in Fig. 5 are linearly independent of the POD basis components and thus span a different subspace. Note also that their influence is not only significant in the vicinity of the cylinder but mostly in its wake.

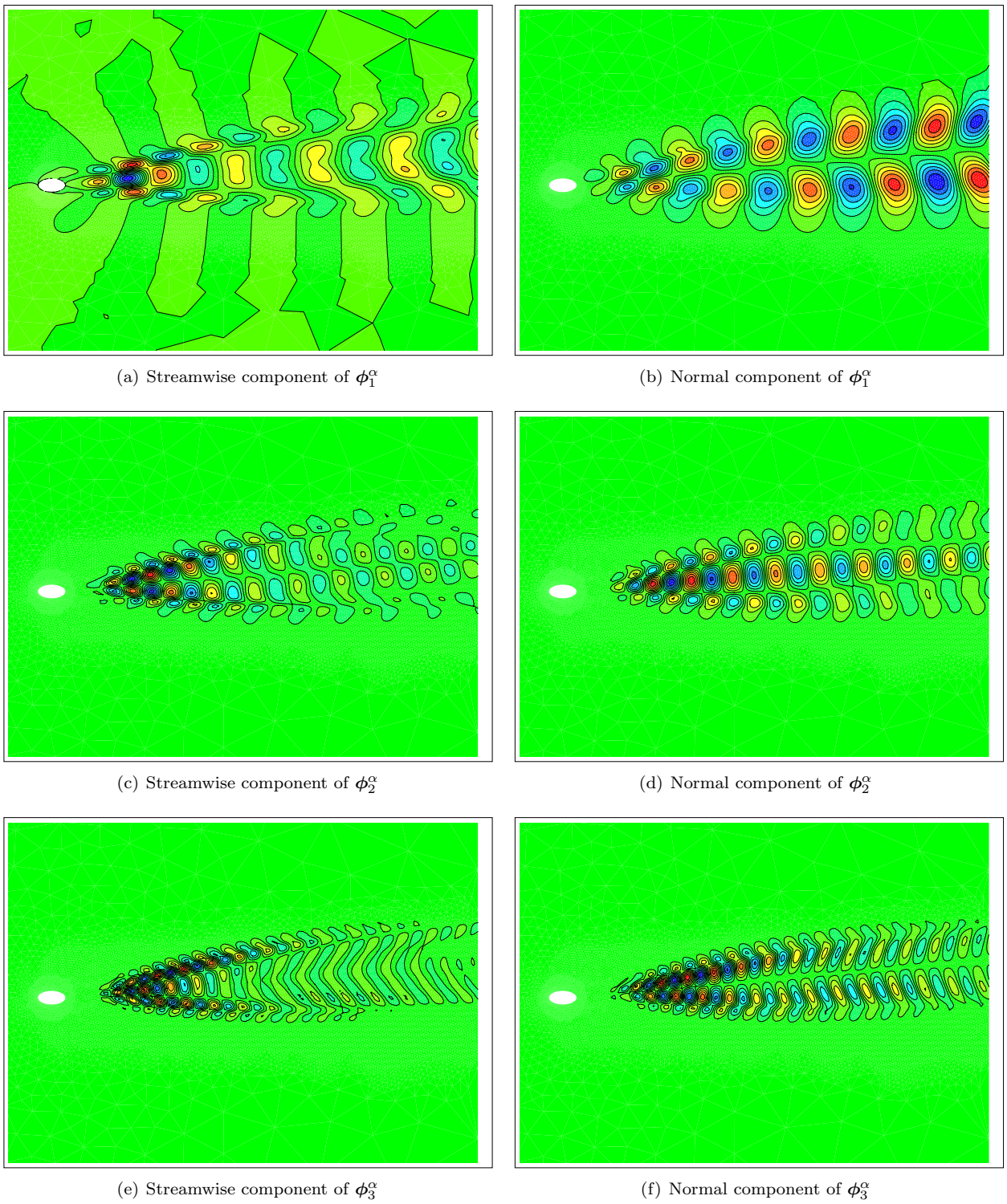

(a) Streamwise component of $\boldsymbol{\phi}_1^{\alpha}$

(b) Normal component of $\boldsymbol{\phi}_1^{\alpha}$

(c) Streamwise component of $\boldsymbol{\phi}_2^{\alpha}$

(d) Normal component of $\boldsymbol{\phi}_2^{\alpha}$

(e) Streamwise component of $\boldsymbol{\phi}_3^{\alpha}$

(f) Normal component of $\boldsymbol{\phi}_3^{\alpha}$

Figure 5. Iso-lines of the components of three baseline POD sensitivity modes

B. Reduced-order approximations

This section reports the performance of reduced-order approximations and models built from the bases described in Section IV for the short term dynamic of flows. To focus on the influence of the basis used in the reduced-order modeling, all ROM simulations are initialized using the DNS data at the considered state and use the appropriate centering (note, however, that in the context of the extrapolated idea, the mean flow can be extrapolated using the sensitivity of the mean flow which is easily calculated from the flow sensitivities at the baseline; and for the expanded approach, the low-dimensional basis can be expanded by the sensitivity of the mean flow to take into account the mean flow modification through parameter changes; the interested reader is referred to 9 for details.) We compare the low-dimensional solutions (referred to as *ROM*) to the full-order solution obtained by a finite-element calculation at the perturbed state. We also look at the error in the low-order approximations where the time coefficients are obtained by projection on the DNS data (referred to as *POD*). Figure 6 reports errors for bases of dimension 6, 12 and 24. As can be

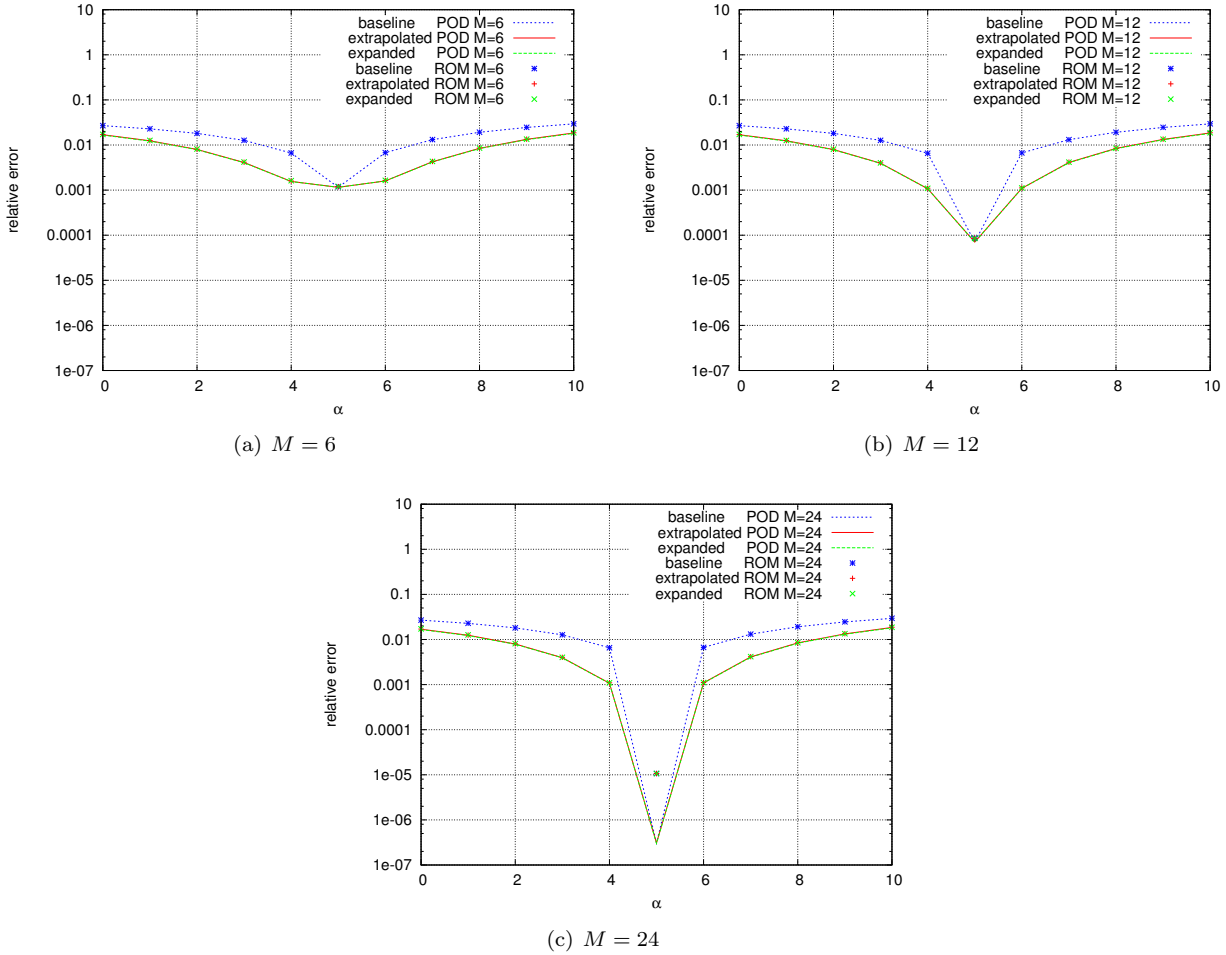

(a) $M = 6$ (b) $M = 12$

(c) $M = 24$

Figure 6. Iso-lines of the components of three baseline POD modes

seen, the two sensitivity-based bases provide better approximations than the baseline basis. This is true for all parameter perturbations but the best improvements are obtained around the baseline as expected. At the baseline, all bases perform the same (for a fixed dimension) since they all contain at least the first M POD modes at this state. The baseline and extrapolated bases are the same and only the expanded basis is different due to the additional POD mode sensitivities. This result shows that the baseline sensitivity modes do not represent a significant part of the energy in the baseline data and that the POD modes alone provide an efficient low-dimensional basis for the baseline flow. However, when one moves away from the baseline state, the baseline POD basis loses its ability to approximate flow solutions so that the baseline approach becomes inaccurate. At these points, the mode sensitivities provide relevant directions to account

for perturbations in solutions due to parameter changes. Close to the baseline, this additional information is enough to yield representation errors as low as for the perturbed basis. When one goes further from the baseline in the parameter space this is no longer true. This means that for large parameter perturbations, the first-order POD mode sensitivities can not account for all changes in the solutions. However, at these states, the extrapolated and expanded bases provide better approximations than the baseline basis.
It is worth noting that errors in low-order approximations obtained by projection (POD) or by solving a dynamical system (ROM) are the same (except for $M = 24$ at the baseline). It shows that these ROM capture the dynamics of their basis components well.
More surprisingly, the extrapolated and expanded approaches yield approximations of similar accuracy for all parameter values. This is in contradiction with previous studies where the expanded approach has performed significantly better for large parameter changes and thus was considered a more robust approach far away from the baseline.

VI. Acknowledgments

This research was partially supported by the Air Force Office of Scientific Research under contract FA9550-08-1-0136. Numerical simulations were performed on Virginia Tech Advanced Research Computing - System X. The allocation grant and support provided by the staff are also gratefully acknowledged.

References

[1]Bakewell, H. P. and Lumley, J. L., "Viscous sublayer and adjacent wall region in turbulent pipe flow," *The Physics of Fluids*, Vol. 10, No. 9, 1967, pp. 1880–1889.

[2]Holmes, P., Lumley, J. L., and Berkooz, G., *Turbulence, Coherent Structures, Dynamical Systems and Symmetry*, Cambridge University Press, Cambridge, UK, 1996.

[3]Sirovich, L., "Turbulence and the dynamics of coherent structures," *Quarterly of Applied Mathematics*, Vol. 45, 1987, pp. 561–590.

[4]Deane, A. E., Kevrekidis, I. G., Karniadakis, G. E., and Orsag, S. A., "Low-dimensional models for complex geometry flows: Application to grooved channels and circular cylinder," *Physics of Fluids A*, Vol. 3, No. 10, 1991, pp. 2337–2354.

[5]Ma, X. and Karniadakis, G., "A low-dimensional model for simulating three-dimensional cylinder flow," *Journal of Fluid Mechanics*, Vol. 458, 2002, pp. 181–190.

[6]Williamson, C. H. K., "Vortex dynamics in the cylinder wake," *Annual Review of Fluid Mechanics*, Vol. 28, 1996, pp. 477–539.

[7]Noack, B. R., Afanasiev, K., Morzynski, M., and Thiele, F., "A hierarchy of low-dimensional models for the transient and post-transient cylinder wake," *Journal of Fluid Mechanics*, Vol. 497, 2003, pp. 335–363.

[8]Hay, A., Borggaard, J., and Pelletier, D., "On the use of Sensitivity Analysis to Improve Reduced-Order Models," *4th AIAA Flow Control Conference*, Seattle, Washington, June 2008, AIAA-2008-4192.

[9]Hay, A., Borggaard, J. T., and Pelletier, D., "Local improvements to reduced-order models using sensitivity analysis of the proper orthogonal decomposition," *Journal of Fluid Mechanics*, Vol. 629, 2009, pp. 41–72.

[10]Hay, A., Borggaard, J., and Pelletier, D., "Reduced-Order Models for parameter dependent geometries based on Shape Sensitivity Analysis of the POD," *12th AIAA/ISSMO Multidisciplinary Analysis and Optimization Conference*, Victoria, British Columbia, September 2008, AIAA-2008-5962.

[11]Hay, A., Borggaard, J., Akhtar, I., and Pelletier, D., "Reduced-Order Models for Parameter Dependent Geometries based on Shape Sensitivity Analysis," *Journal of Computational Physics*, Vol. 229, 2010, pp. 1327–1352.

[12]Akhtar, I., Hay, A., Borggaard, J., and Iliescu, T., "Sensitivity analysis-based reduced-order models for flow past an elliptic cylinder," *Proceedings of the 47th Aerospace Sciences Meeting and Exhibit*, AIAA Paper No. 2009-0583, 2009.

[13]Akhtar, I., Borggaard, J., and Hay, A., "Shape Sensitivity Analysis in Flow Models using a Finite-Difference Approach," *to appear in Mathematical Problems in Engineering*, 2010.

[14]Noack, B. R., Papas, P., and Monkewitz, P. A., "The need for a pressure-term representation in empirical Galerkin models of incompressible shear flows," *Journal of Fluid Mechanics*, Vol. 523, 2005, pp. 339–365.